

## Infrared Thermography on the COMPASS Tokamak

P. Vondráček,<sup>1,2</sup> J. Horáček,<sup>1</sup> P. Cahyna,<sup>1</sup> R. Pánek,<sup>1</sup> J. Uličný<sup>3</sup>

<sup>1</sup>Institute of Plasma Physics AS CR, v.v.i., Association EURATOM/IPP.CR, Prague, Czech Republic.

<sup>2</sup>Charles University in Prague, Faculty of Mathematics and Physics, Prague, Czech Republic.

<sup>3</sup>Czech Technical University in Prague, Faculty of Nuclear Sciences and Physical Engineering, Prague, Czech Republic.

**Abstract.** This contribution describes some aspects of calibration and experimental operation of a slow infra-red camera used at the COMPASS tokamak at IPP Prague. We focus on the camera limitations affecting the experimental data (mainly temporal smoothing). Data time deconvolution used to correct the effect of the long response time of the camera detector is described. Smaller part of the contribution is devoted to the design of a fast IR camera system planned for installation in COMPASS in 2014.

### Introduction

The COMPASS tokamak is equipped by a quite large set of diagnostics. A slow bolometric infrared (IR) camera was installed in the late 2012. The camera provides information about temperature of solid surfaces and their heat loads, so it is useful for plasma facing components monitoring as well as for plasma surface interaction physics studies. First experiment using the IR camera was performed in last months — it is briefly described in the next section. It was necessary to perform camera calibration and some signal corrections before the experiment — this procedure is described in following sections.

### Motivation — HFS limiter heat load studies in support of ITER

Recent observations on JET [Arnoux et al., 2013] have revealed unexpected power loading features near the last closed flux surface on inner wall limiters, characteristic either of a narrow *parallel heat flux characteristic decay length* ( $\lambda_q$ ) in the near scrape-off layer (SOL), or the presence of a cross-field *funneling effect*, suggested as an explanation for similar observations two decades ago on TFTR [Stangeby et al., 1992]. Such narrow SOLs are not accounted for in the design of the ITER first wall (FW) panels, which are shaped to protect against misalignments and which have a similar roof-shaped design to that employed on the JET central column limiters. With the ITER FW at the final design review phase, further detailed study of this issue is urgently required to assess whether the start-up power handling will be sufficient. A series of dedicated experiments have thus been performed on the COMPASS tokamak, in which specially designed inner wall graphite tiles have been installed at a single toroidal location on the central column.

The limiter heat load distribution was calculated using the THEODOR code [Herrmann et al., 1995] from the data measured by the slow IR camera. The required radial profile of a parallel heat flux in a SOL was extracted using EFIT reconstruction of magnetic surfaces and heat flux asymmetry with an effect of plasma current ( $I_p$ ) direction were observed. Preliminary results of the experiment were presented in Vondracek et al. [2013].

It was necessary to calibrate the camera and to correct long response time of the camera detector for the purpose of the experiment. Some aspects of this procedure are described in this article.

### Thermal Infrared Detector Principles

The heart of each IR camera is its detector. In our case it is focal plane array (FPA) of 160x120 small bolometers converting incoming photon flux to electric signal thanks to change of its temperature and consequently resistivity. Response of each bolometer (typically voltage signal) is a linear function of temperature difference  $\Delta T$  between bolometer and detector substrate (heat sink at constant temperature) for small  $\Delta T$

$$X(\Delta T) \sim R(T_s)[1 + \alpha\Delta T]. \quad (1)$$

$\alpha$  is *temperature coefficient of resistance*,  $T_s$  is temperature of the substrate,  $R$  is resistivity [Kruse and Skatrud, 1997]. Temperature increase  $\Delta T$  is described by a heat balance equation

$$c \frac{d\Delta T}{dt} + g_{\text{leg}} \Delta T + P_{\text{rad}} = \varepsilon P_{\text{obj}} + \varepsilon P_s + P_j, \quad (2)$$

where  $c$  is bolometer heat capacity,  $g_{\text{leg}}$  thermal conductance of a support structure (connection to the substrate),  $\varepsilon$  emissivity,  $P_{\text{rad}}$  radiation power emitted by the bolometer,  $P_{\text{obj}}$  radiation power incoming from an observed object,  $P_s$  radiation power incoming from the substrate,  $P_j$  joule power produced by applied bias of IR camera circuitry — see Kruse and Skatrud [1997], ch. 3/II.3 and Rogalski [2010].

Radiation power emitted by the bolometer can be expressed using Stefan-Boltzman's law

$$P_{\text{rad}} = \varepsilon (2A) \sigma T^4 \approx \varepsilon (2A) \sigma T_s^4 + 4\varepsilon (2A) \sigma T_s^3 \Delta T = k_0 + g_{\text{rad}} \Delta T, \quad (3)$$

where we assume, that  $\Delta T$  is small enough and bolometer is very thin layer of sensitive material with collecting area  $A$ , so that  $2A$  is its total surface area.  $k_0$  is a constant equal to the bolometer radiation at substrate temperature. Radiation power incoming from an observed object is given by the Planck's law

$$P_{\text{obj}} = \varepsilon k_1 \Phi(T_{\text{obj}}) = \varepsilon k_1 \int_{\lambda_1}^{\lambda_2} \frac{2hc^2}{\lambda^5} \frac{1}{e^{\frac{hc}{\lambda k_B T_{\text{obj}}}} - 1} d\lambda, \quad (4)$$

where  $k_1$  is a constant and  $\Phi(T_{\text{obj}})$  is radiation intensity of ideal black body at the same temperature as observed object.  $\lambda_1$  and  $\lambda_2$  are spectral range boundaries of the camera — in our case 7 and 13.5  $\mu\text{m}$ . We can replace radiation power incoming from the substrate by a constant, thanks to its constant temperature. For simplicity we will assume joule power produced by applied bias to be also constant. Simplified heat balance equation is then

$$c \frac{d\Delta T}{dt} = \varepsilon k_1 \Phi(T_{\text{obj}}) - g \Delta T + k_2, \quad (5)$$

where  $g = g_{\text{leg}} + g_{\text{rad}}$  is *total thermal conductance*,  $k_1$  and  $k_2$  are constants.

Temperature output of the camera is extracted from the stationary solution of the eq. (5)

$$\Delta T = \frac{\varepsilon k_1}{g} \Phi(T_{\text{cam}}) + \frac{k_2}{g}, \quad (6)$$

so that camera output is

$$T_{\text{cam}} = \Phi^{-1} \left[ \frac{g}{\varepsilon k_1} \Delta T - \frac{k_2}{\varepsilon k_1} \right]. \quad (7)$$

Camera signal is disturbed for fast events thanks to the omission of the time derivative in the eq. (5) for camera output extraction (eq. (7)). Correct solution of the eq. (5) for a step signal of  $\Phi$  ( $\Phi = 0$  for  $t < 0$  and  $\Phi = Q$  for  $t > 0$ ) for  $t > 0$  is

$$T(t) = T_s + \frac{Q}{g} \left[ 1 - e^{-t/\tau} \right]. \quad (8)$$

Microbolometer temperature responds to IR power with an exponential *thermal response time*

$$\tau = \frac{c}{g}. \quad (9)$$

Thermal response time should be much lower than time interval between 2 frames of a camera — but this is not the case of our camera, as is described in the next section.

Combining eq. (5) and (6) one can obtain correct temperature of an observed object as

$$T_{\text{obj}} = \Phi^{-1} \left[ \Phi(T_{\text{cam}}) + \frac{c}{g} \frac{\partial \Phi}{\partial T}(T_{\text{cam}}) \frac{\partial T_{\text{cam}}}{\partial t} \right] \quad (10)$$

Another possible way how to obtain real temperature of an observed object is to write eq. (5) in an operator form as

$$\hat{L} \Delta T = \frac{\varepsilon k_1}{c} \Phi(T_{\text{obj}}) + \frac{k_2}{c}, \quad (11)$$

where

$$\hat{L} \equiv \frac{d}{dt} + \frac{g}{c}. \quad (12)$$

Solution of the eq. (11) could be expressed as a convolution

$$\Delta T = \left[ \frac{\varepsilon k_1}{c} \Phi(T_{\text{obj}}) + \frac{k_2}{c} \right] * G \quad (13)$$

of the right side with a Green's function  $G$

$$G(t < 0) = 0 \wedge G(t \geq 0) = e^{-t/\tau}. \quad (14)$$

Temperature of an observed object is then

$$T_{\text{obj}} = \Phi^{-1} \left[ \text{deconvolution} \left( \frac{c}{g} \Phi(T_{\text{cam}}), G \right) \right] \quad (15)$$

## Camera calibration

The COMPASS tokamak is equipped by the Micro-Epsilon TIM160 camera. The detector of the camera is uncooled microbolometer with  $160 \times 120$  px. and frame-rate 120 Hz. Four different temperature ranges could be used — altogether covering region from  $-20$  °C up to  $1500$  °C. Noise equivalent temperature difference (NETD) of the camera is  $0.3$  K. Camera accuracy is  $\pm 2$  °C or  $\pm 2$  % (whichever is greater).  $35.5$  mm lens with  $6^\circ \times 5^\circ$  field of view (FOV) is used.

**NUC and BPR.** The detector response is not uniform (slightly differs for each pixel) and one needs to perform *Non Uniformity Correction* (NUC). The best way is to expose all the bolometers to the same temperature using a black body with extensive surface area or placed close to the lens of the camera (in an unfocused area). The response of each detector should be then corrected to equal the mean value  $\bar{X}$  of response of whole array

$$X_{ij \text{ corrected}} = \alpha_{ij} X_{ij} + \beta_{ij} = \bar{X}, \quad (16)$$

where  $\alpha_{ij}$  is detector *gain* and  $\beta_{ij}$  is *offset*.

Bad/damaged pixels could be replaced by some of their neighbors. This routine is called *Bad Pixel Replacement* (BPR). There are several ways, how to determine the list of bad pixels. First method is to fix some range for the gain — pixels exceeding this range are considered to be bad pixels. The same could be done for the offset. Another way is to define a limit for a time noise level.

These calibrations for our camera with  $35.5$  mm lens were made by camera manufacturer.

**Temperature calibration.** Detector response is non-linear function of temperature of observed object. One needs to perform a temperature calibration of the detector response — the simplest way is to use calibration black body with adjustable temperature.

**Optical path calibration.** Ideal black body absorbs all incoming radiation in contrast to real objects, which absorb only part of the radiation and the rest is transmitted or reflected. These phenomena are described by *absorptivity*  $\alpha$ , *transmissivity*  $\tau$  and *reflectivity*  $\varphi$ . Ratio of object's own thermal radiation to that of ideal black body with the same temperature is determined by *emissivity*  $\varepsilon$ , which is equal to absorptivity and thus

$$\varepsilon + \tau + \varphi = 1. \quad (17)$$

It is necessary to know these coefficients for all optical elements used for IR measurement and compensate response of a detector to obtain correct temperature.

Our optical path consists of camera lens and one  $4$  mm thick ZnSe vacuum window. We performed optical path calibration together with temperature calibration using calibration black body in the range  $25$ – $400$  °C — the procedure was described in Ulicny [2013]. Emissivity of the graphite limiter observed during the experiments was measured using calibration sticker with known emissivity ( $0.95$ ) placed on the limiter. It was found that limiter has emissivity in the range  $0.95$ – $1$ .

**Long thermal response time correction.** Measuring heat flux load to the limiter tile after plasma disruption (sudden end of a plasma discharge) we observed that characteristic thermal response time of our IR camera is quite long — comparable with the frame-rate. This was confirmed by a simple experiment with rectangular heat pulse using soldering iron as a heat source and covering the camera detector by a thick cardboard. Soldering iron image was still visible a few frames after the detector had been covered, as can be seen in Fig. 1. Fitting time evolution of radiation intensity calculated from temperature signal of 1 pixel we obtained response time  $\tau \approx 9$  ms.

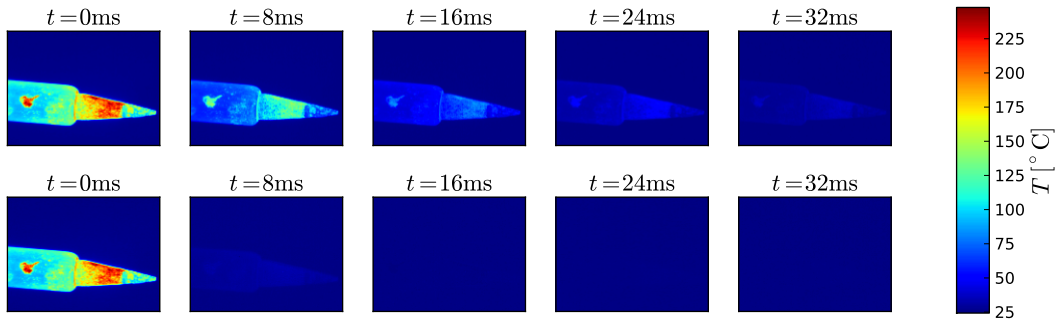


**Figure 1.** Comparison of the original (first row) and deconvoluted temperature signal (second row). Camera detector was covered between first 2 frames (in the time  $0 \text{ ms} < t < 8 \text{ ms}$ ).

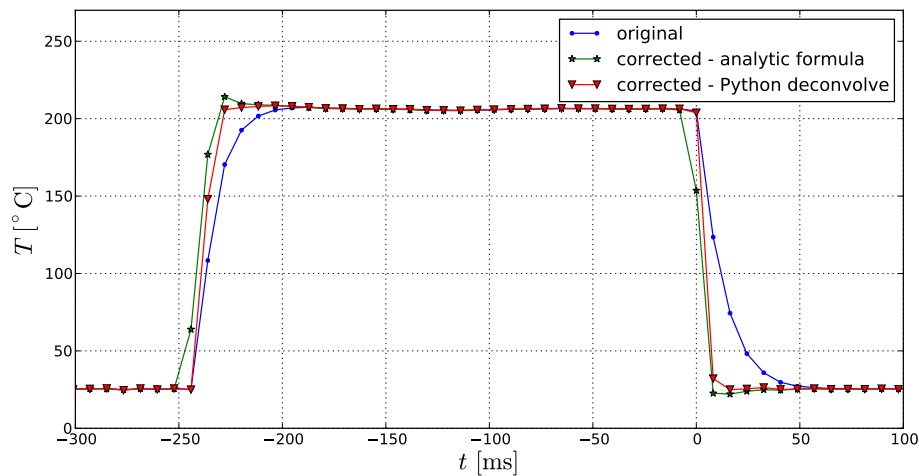


**Figure 2.** Comparison of the camera temperature signal — original, deconvoluted using eq. (10) and deconvoluted using eq. (15) together with Python `deconvolve` routine. Deconvolution using eq. (10) strongly depends on numerical differentiation used for the calculation — central difference is used here.

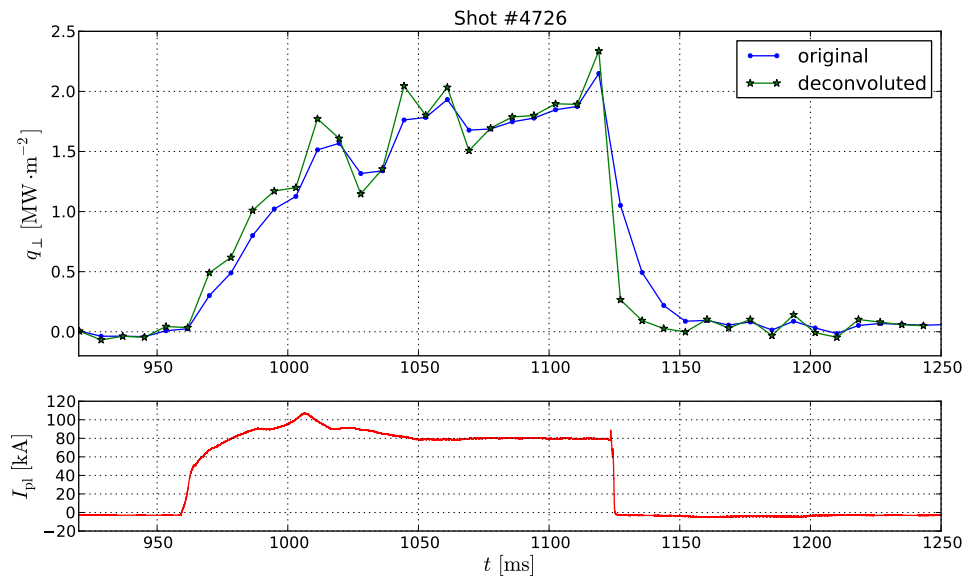


**Figure 3.** Time evolution of the heat flux to the inner limiter of the COMPASS tokamak during plasma discharge calculated from IR camera temperature signal (original and deconvoluted) by the means of the THEODOR code. The plasma shot was disrupted at approx.  $t = 1125 \text{ ms}$  (as you can see in the plasma current signal), so the heat flux should fall down to zero value immediately.

We performed time deconvolution to correct signal of the camera for the response time. It is necessary to convert temperature signal to radiation intensity and vice versa for this purpose — to integrate the Planck’s law and find an inverse function for all the data points, which is quite computationally intensive. So we built 2 *look-up* tables — for time to radiation intensity conversion and vice versa — with a step of  $10^{-2}$  K and  $\text{Wm}^{-2}$  respectively.

Deconvoluted rectangular signals for 1 pixel calculated numerically in terms of the eq. (10) as well as calculation using built-in Python `deconvolve` function in terms of the eq. (15) are shown in Fig. 2. Comparison of a heat flux calculated directly from the camera temperature signal and from the deconvoluted signal for the inner wall limiter heat load experiments at the COMPASS tokamak is shown in Fig. 3.

## COMPASS fast IR camera design plan

One of the main experimental areas of interest of the COMPASS tokamak in the next years are studies of resonant magnetic perturbations (RMP) using a quite complex set of saddle coils. The key effect of RMPs applied externally to a tokamak plasma is creation of magnetic islands and resulting ergodization of magnetic field lines leading to disturbance of a steep temperature and density radial profile (so called *pedestal*) just inside the last closed flux surface (LCFS) in high confinement tokamak operation mode (*H-mode*). RMPs are promising tool to control type-I edge localized modes (ELMs), which carry large amount of energy out of the plasma and are critical phenomenon for ITER and a future fusion power plant. Effects associated with the RMP ELM mitigation techniques were studied at a few other tokamaks as DIII-D, JET or MAST and COMPASS should provide extension of present experience to wider range of parameters thanks to its similar geometry and smaller dimensions. Coils to induce RMPs for ELM mitigation are proposed in the ITER design [Lang et al., 2013]. There are however still many open questions concerning the mechanism itself and related issues, and the theory of the mitigation effect is far from being completely understood.

Calculations of spectra of RMPs caused by saddle coils were performed using ERGOS code as a part of preparations for COMPASS RMP experiment, with the objective of determining the magnetic island width and the extent of ergodic regions [Cahyna et al., 2009]. Expected splitting of divertor strike points (regions of main plasma-surface interaction on a divertor), which are the crucial consequence of RMP, was calculated in Cahyna and Nardon [2011] — an example is shown in Fig. 4.

The ideal instrument for divertor strike point spectroscopy for the COMPASS tokamak is under development. The camera system for the COMPASS tokamak is under development and should be installed in 2014. The camera will observe the upper vessel port with a pixel size  $\approx 0.6$  mm and a frame rate of 20 kHz. The camera should provide frame-rate  $\geq 20$  kHz. The camera should be able to reach very short integration times (less than thermal response time of a bolometer).

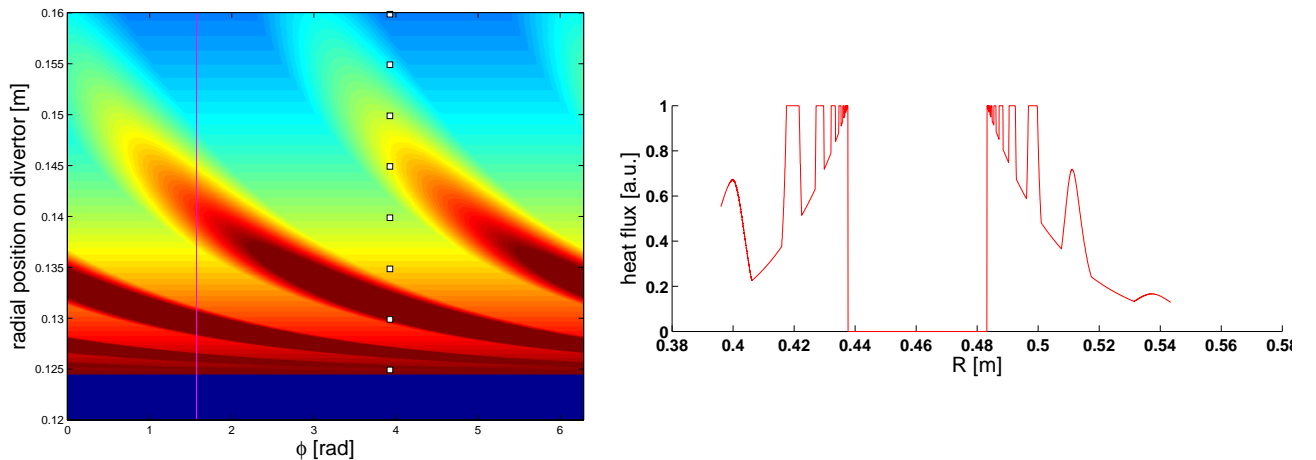


**Figure 4.** Left — modeled top view of outer strike point divertor region during RMP operation. Right — expected radial profile of heat flux to the divertor.

## Conclusion

The infra-red thermography is a new promising diagnostics at the COMPASS tokamak. A slow bolometric IR camera is available at the moment, all necessary calibration routines were performed as well as correction of the long thermal response time of the camera detector.

The fast IR camera system is being designed and will contribute to the future experimental studies at the COMPASS tokamak, mainly concerning RMP and ELM physics.

**Acknowledgments.** The work was supported in part by Grant Agency of the Czech Republic under Grant No. P205/11/2341 and MSMT Project No. LM2011021

## References

- Arnoux, G., Farley, T., Silva, C., Devaux, S., Firdaouss, M., Frigione, D., Goldston, R. J., Gunn, J., Horacek, J., Jachmich, S., Lomas, P. J., Marsen, S., Matthews, G. F., Pitts, R. A., Stamp, M., Stangeby, P. C., and JET-EFDA Contributors, Scrape-off layer properties of ITER-like limiter start-up plasmas in JET, *Nuclear Fusion*, *53*, 073016, 2013.
- Cahyna, P. and Nardon, E., Model for screening of resonant magnetic perturbations by plasma in a realistic tokamak geometry and its impact on divertor strike points, *Journal of Nuclear Materials*, *415*, S927 – S931, proceedings of the 19th International Conference on Plasma-Surface Interactions in Controlled Fusion, 2011.
- Cahyna, P., Panek, R., Fuchs, V., Krlin, L., Becoulet, M., Huysmans, G., and Nardon, E., The optimization of resonant magnetic perturbation spectra for the COMPASS tokamak, *Nuclear Fusion*, *49*, 055024, 2009.
- Herrmann, A., Junker, W., Gunther, K., Bosch, S., Kaufmann, M., Neuhauser, J., Pautasso, G., Richter, T., and Schneider, R., Energy flux to the ASDEX-Upgrade divertor plates determined by thermography and calorimetry, *Plasma Physics and Controlled Fusion*, *37*, 17, 1995.
- Kruse, P. W. and Skatrud, D. D., *Uncooled infrared imaging arrays and systems*, no. sv. 47 in *Semiconductors and Semimetals*, Academic Press, 1997.
- Lang, P. T., Loarte, A., Saibene, G., Baylor, L. R., Becoulet, M., Cavinato, M., Clement-Lorenzo, S., Daly, E., Evans, T. E., Fenstermacher, M. E., Gribov, Y., Horton, L. D., Lowry, C., Martin, Y., Neubauer, O., Oyama, N., Schaffer, M. J., Stork, D., Suttrop, W., Thomas, P., Tran, M., Wilson, H. R., Kavin, A., and Schmitz, O., ELM control strategies and tools: status and potential for ITER, *Nuclear Fusion*, *53*, 043004, 2013.
- Rogalski, A., *Infrared Detectors, Second Edition*, Taylor & Francis, 2010.
- Stangeby, P. C., Pitcher, C. S., and Elder, J. D., The nature of plasma fluxes to surfaces nearly tangential to the magnetic field, *Nuclear Fusion*, *32*, 2079, 1992.
- Ulicny, J., *Calibration of infrared camera on tokamak COMPASS*, Bachelor thesis, Faculty of Nuclear Sciences and Physical Engineering, Czech Technical University in Prague, 2013.
- Vondracek, P., Horacek, J., Panek, R., Pitts, R. A., Stangeby, P. C., Goldston, R. J., Kocan, M., Arnoux, G., Pipek, J., Janky, F., Havlicek, J., Imrisek, M., Hacek, P., and Hron, M., COMPASS inner wall limiter heat load physics studies in support of ITER, poster P1.116 at EPS conference in Helsinki (Finland), 2013.